Solid-State Electronics 54 (2010) 22–27

Contents lists available at ScienceDirect

Solid-State Electronics

journal homepage: www.elsevier.com/locate/sse

A comparative study of photoconductivity and carrier transport in a-Si:H p–i–n solar cells with different back contacts

R. Kaplan [a,*], B. Kaplan [a], S.S. Hegedus [b]

[a] Department of Secondary Science and Mathematics Education, University of Mersin, Yenisehir Campus, 33169 Mersin, Turkey
[b] Institute of Energy Conversion, University of Delaware, Newark, DE 19716, USA

ARTICLE INFO

Article history:
Received 22 September 2008
Received in revised form 3 August 2009
Accepted 8 September 2009
Available online 9 October 2009

The review of this paper was arranged by Prof. S. Cristoloveanu

Keywords:
a-Si:H p–i–n solar cells
Back reflectors
Photocurrent
Quantum efficiency
Recombination
Trapping

ABSTRACT

Effects of different back contacts (Al, Cr, ZnO/Ag, Ag) have been measured on hydrogenated amorphous silicon (a-Si:H) p–i–n solar cell performances and are interpreted in terms of changing recombination kinetics. Dc and frequency-resolved photocurrent measurements in a-Si:H p–i–n solar cells have been carried out experimentally. In particular, the *J–V* characteristics in the dark and light, the external quantum efficiency spectra, the intensity-, temperature-, bias voltage- and frequency-dependence of photocurrent were obtained. Fill factor (*FF*) values were determined from *J–V* characteristics for p–i–n cells with different back contacts under various illumination levels. The exponent ν in the power-law relationship, $I_{ph} \propto G^{\nu}$, between generating flux density and photocurrent were determined at different bias voltages (dc) and modulation frequencies. The activation energies were obtained from the temperature-dependence of photocurrent measurements. The integrated external quantum efficiencies were calculated from the spectral photoresponse distributions under reverse bias conditions. The modulation-frequency effects on spectral distributions were also investigated. The results were compared for all cells which have different back contacts and excitation intensity.

© 2009 Elsevier Ltd. All rights reserved.

1. Introduction

In recent years electricity generation from renewable resources has been counted upon to bridge the gap between global demand and supply of power. Solar has good potential and the direct conversion technology based on solar photovoltaics has several positive attributes [1–3].

The main research activities in the photovoltaic field are related to materials development, which can be obtained at relatively low cost and to improve the conversion efficiency [4–7]. Owing to its many exciting technological applications, hydrogenated amorphous silicon, a-Si:H, became the most intensively studied amorphous semiconductor [8,9].

The performance of the solar cell was characterized by the *J–V* curves, the frequency-, intensity- and temperature-dependent photocurrent, and the spectral photoresponse. The spectral photoresponse and thus the quantum efficiency have been used to characterize the ability to collect charge carriers generated by different wavelengths of the sun spectrum, which are powerful tools for the development and calibration of solar cells, due to the fact that the light is absorbed differently in each layer, and it allows monitoring the layers properties.

An important parameter for the high efficiency solar cells is that back contacts combine low resistivity with a low recombination velocity for minority carriers and a high optical reflectance in order to enable efficient light trapping [10–12].

The aim of this paper is to optimize the radiation and recombination losses by investigating four types of p–i–n solar cells which have the same a-Si recipe but different back contact materials. The enhancement of the reflection from the rear contact of p–i–n a-Si solar cells using Al, Cr, ZnO/Ag and Ag as a back reflector was demonstrated experimentally. In particular, the effects of using different back contacts on the fill factor *FF*, the external quantum efficiency $QE(-1V)$, the short-circuit current density J_{sc}, and the exponent ν in the intensity-dependent power-law relationship $I_{ph} \propto G^{\nu}$ were investigated and compared.

2. Experimental details

In this work, we used four of samples which are 1×1 in. substrates of a-Si:H p–i–n devices. These devices were obtained from the Institute of Energy Conversion (IEC), University of Delaware. All devices have the same SnO_2 substrates, the same deposition conditions, but different back contacts. The cells have a layer-sequence of glass/TCO/p–i–n/back contact. The back contact material used and *J–V* results for all cells are given in Table 1. These measurements were taken under ≈1 sun illumination by using 4-terminal

* Corresponding author. Tel.: +90 324 3412815x2021; fax: +90 324 3412823.
E-mail address: ruhikaplan@yahoo.com (R. Kaplan).

0038-1101/$ - see front matter © 2009 Elsevier Ltd. All rights reserved.
doi:10.1016/j.sse.2009.09.008

Table 1
Illuminated *J–V* results (AM1.5 global light from an Oriel simulator) for a-Si:H p–i–n solar cells with different back contacts. R_{OC} is the resistance at open circuit. Also shown are values of the *QE* integrated with the AM1.5 spectrum.

Sample	Back contact	V_{oc} (V)	J_{sc} (mA/cm^2)	V_{mp} (V)	J_{mp} (mA/cm^2)	*FF* (%)	R_{OC} (Ω cm^2)	Integrated *QE* (mA/cm^2)
4729-12	Al	0.83	14.79	0.62	11.63	58.6	7.87	14.70
4729-11	Cr	0.84	13.22	0.64	10.56	60.4	9.82	12.90
4729-21	ZnO/Ag	0.86	15.10	0.65	12.79	64.0	6.83	14.80
4743-21	Ag	0.83	15.27	0.57	12.38	55.6	16.77	14.90

configuration due to the high resistance. The cell area is 0.4 cm^2, and the substrate contact is along the side. The i-layer thickness is about 0.5–0.6 μm for all devices.

As seen from the table given above, the values of R_{OC} are almost close each other for the back contacts of Al, Cr and ZnO/Ag, but it is large for Ag back contact. It may be due to different dark current curve obtained in Fig. 1. For the back contacts of Ag and ZnO/Ag, the values of integrated *QE* are larger than those of others due to larger J_{sc} measured.

A HeNe laser (632.8 nm, 0.65 mm beam diameter, 10 mW o/p max.) was used as the excitation light to obtain *J–V* characteristics, intensity- and frequency-dependences of photocurrent. Neutral density filters (NDF) were used to vary the intensity of light incident on the p–i–n solar cell to between 20 μW and 10 mW. The incident light was chopped at the frequencies between 10 Hz and 4 kHz. The modulated signals were detected by pre- and lock-in amplifiers. For dc measurements, an electrometer (Model 6514) was used.

The quantum efficiency (*QE*) was measured from 400 to 750 nm using the same lock-in detection system chopped at 70 Hz, illuminated through a monochromator having 12 nm width at half maximum. The system was calibrated using a filtered (Schott KG5) crystalline Si device as was used to calibrate the Oriel solar simulator.

Only the best results for solar cells with different back contacts (Table 1) are reported in the following.

3. Results and discussion

Fig. 1 shows a comparison of *I–V* characteristics of four p–i–n solar cells with different back contacts. As seen, the reverse bias characteristics are almost the same and close to ideal diode characteristics for all back contacts. However, there is difference between the Ag back contact and others under forward bias condition.

Fig. 2 shows the *I–V* characteristics of Al back contact for various levels of illumination. As well known, the electrical characteristics of a solar cell is described by the relation between the current density *J* (=*I*/*A*, where *I* current, *A* cell area) flowing through the cell and the potential *V* across it, while the cell is illuminated. A convenient way to characterize the electrical performance of a solar cell is to specify its open circuit voltage V_{oc}, its short-circuit current density J_{sc} and its fill factor *FF*. The latter is a measure of the rectangularity of the *J–V* curve and is defined by

$$FF = \frac{V_m J_m}{V_{oc} J_{sc}}, \quad (1)$$

where V_m and J_m are the voltage and current density at the maximum power point respectively, and ($V_m J_m$) is the maximum power per unit of area P_m. The graphical interpretation of P_m is the area of the largest rectangle below the *J–V* curve; ($V_{oc} J_{sc}$) is the area if the curve was a true rectangle. From the definition of *FF*, it follows that $P_m = FF(V_{oc} J_{sc})$. The efficiency of a solar cell η is in fact the efficiency at maximum power delivery, so that $\eta = P_m/P_{in}$, where P_{in} is the incident light intensity. It is clear that any loss in *FF* will reduce the efficiency of the solar cell. One must note that V_{oc}, J_{sc} and *FF* are not the fitting parameters and do not depend on any model describing the solar cells. From the fourth quadrant of Fig. 2, the calculated values of *FF* are also shown in the figure. A comparison of *FF* for different back contacts is given in Fig. 3, as a function of laser power and back

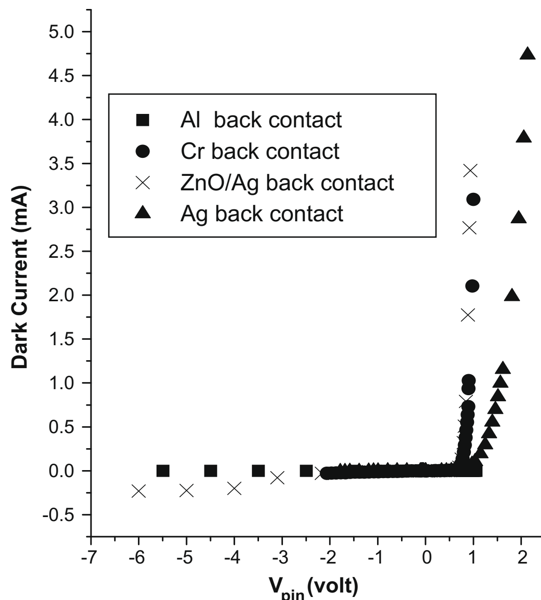

Fig. 1. A comparison of dark *I–V* characteristics (dc) of four a-Si:H p–i–n solar cells which have different back contacts.

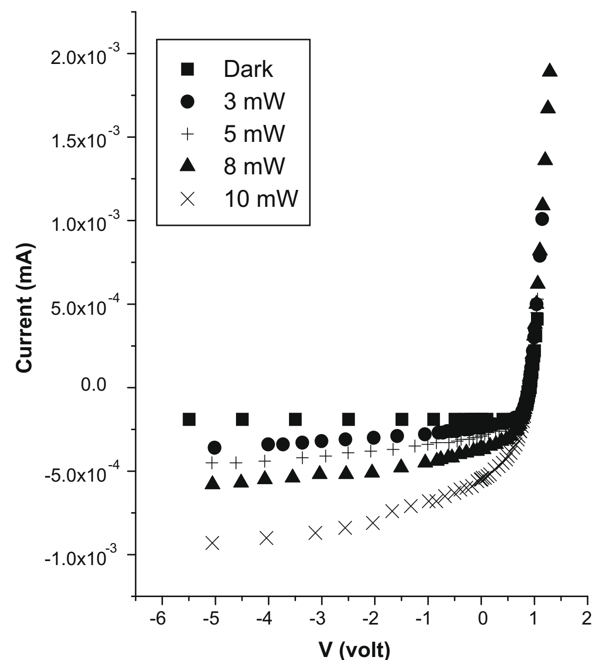

Fig. 2. *I–V* characteristics (dc) of a-Si:H p–i–n solar cell with Al back contact in dark and under various illumination levels.

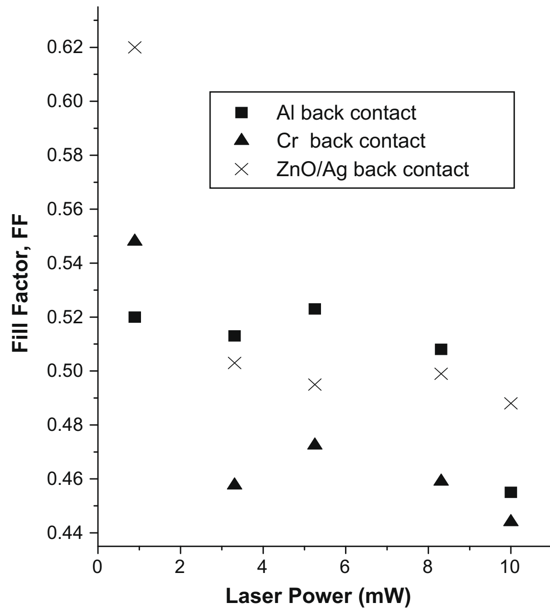

Fig. 3. A comparison of fill factor, *FF*, as a function of laser power for a-Si:H p–i–n solar cell with different back contacts.

contact type. As seen, there is a decrease in *FF* at low powers (⩽3 mW). However, above this power, the *FF* increases gradually with increasing powers, and then it decreases slowly again. The values of *FF* are large at low powers (<1 mW) due to high recombinations. Obviously, the *FF* for Al and ZnO/Ag back contacts is higher than that of Cr back contact. The small value of *FF* may be due to the high excitation intensity used [13]. According to a model proposed by Crandal [14], for the weakly absorbed light, the shape of *J–V* curve is completely specified by electron and hole drift lengths.

Fig. 4 shows a comparison of the short-circuit current densities, J_{sc}, as a function of laser power for three back contacts. As seen, the J_{sc} is the highest for the ZnO/Ag back contact. However it is the lowest for the Al back contact. However, J_{sc} has a linear dependence on intensity for all back contacts as expected.

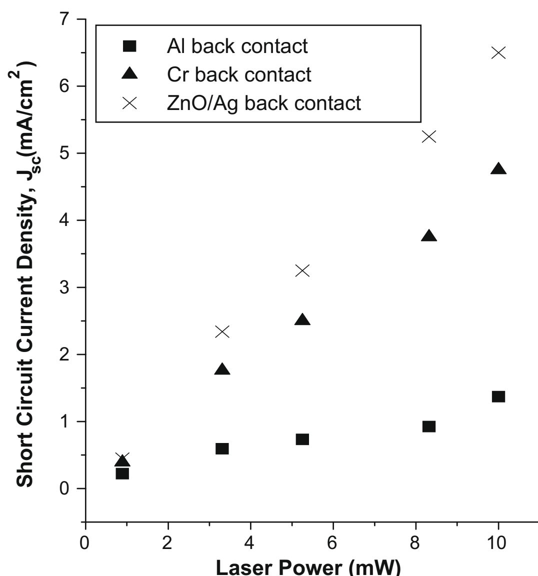

Fig. 4. A comparison of short-circuit current, J_{sc}, as a function of laser power for a-Si:H p–i–n solar cells with different back contacts.

An important feature of the transport properties of amorphous semiconductors such as a-Si:H p–i–n and chalcogenide glasses is the recombination of photogenerated charge carriers via recombination centers. This affects the photocurrent, as well as being of importance for device applications of such materials. The recombination usually occurs through the intermediary of the impurity or defect levels in the gap. In general, these levels correspond to localized electronic states and act as “traps” for the electrons or holes in the band states. When a carrier makes a transition and is trapped at these localized levels, it no longer contributes to the conductivity. However, the carrier can be released and return to the band. If the probability, for recombination, at the level, with a carrier of the opposite sign, is greater than the probability of release to the band, the level is called a recombination center. Conversely, if the probability for release is greater than recombination, the level is simply called a trap. The distinction is mainly based on the proximity of the level to the band edge.

The recombination process comprises mainly two sequential steps in which electrons and holes can recombine so as to reestablish the equilibrium that has been distributed by photoexcitation. The excited electron or hole first loses energy by many transitions within the band, in which the energy decrements are small and frequent. This process is known as thermalization. The thermalization rate decreases as the electron moves into the localized band-tail states and the density of available states is lower. Eventually the electron completes the recombination by making a transition to a hole with the release of a large energy. Recombination lifetimes are generally much longer than the thermalization times, so that the two processes usually takes places on distinctly different time skales. Recombination at low temperatures mostly occurs by tunnelling, because there is not sufficient thermal energy to excite carriers from the band-tail states to the mobility edge. Thermal excitation becomes significant at higher temperatures and changes the recombination mechanisms.

Measurement of photocurrent as a function of excitation light intensity, temperature, wavelength, modulation frequency and applied electric field provides valuable information on the transport properties of photocarriers. The dependence of photocurrent I_{ph} on the photogeneration rate G (which is linearly proportional to the incident light intensity) is given by the power-law,

$$I_{ph} \propto G^{v}. \tag{2}$$

It is differentially defined by

$$v = \frac{d\ln(I_{ph})}{d\ln(G)}. \tag{3}$$

It is now well-known that the value of the exponent v differs in various semiconductors and has quite complicated variations with temperature, applied electric field, photon frequency and light intensity [15–17]. It is common practice to attribute v between 0.5 and 1.0 to a mixture of two limiting recombination mechanisms [18]: a monomolecular recombination type occurring through recombination centers (dangling bonds, midgap, localized levels) which would correspond to $v \approx 1.0$ and a bimolecular recombination process, in which the excess charge carriers recombine directly from the band tails ($v \approx 0.5$). An alternative model proposed by Rose [19] considers an exponential distribution of density of states (DOS) whose states are increasingly converted from trapping to recombination states as the light intensity increased. Different v values between 0.5 and 1.0 are obtained from this model, which depend upon the slope of DOS being swept by the steady state Fermi level, and on temperature. In past, the analytical work on photoconductivity in a-Si:H by Bube [20] demonstrated that a relative simple model for recombination via dangling bonds may produce superlinear photocurrent ($v > 1$) in

undoped material. On the other hand, a sublinear characteristics with exponent ν as low as 0.4 has been observed by numerous groups [21–23]. However, a complete model covering the modulation frequency-dependence of ν has not emerged.

Fig. 5 shows a comparison of the exponent ν as a function of modulation frequency for four back contacts. As seen, there is no strong dependence of ν on the modulation frequency. However, ν values are larger ($\nu > 1$) for Cr and ZnO/Ag back contacts than those of Al and Ag back contacts ($\nu < 1$) on the whole modulation frequency range.

Fig. 6 shows the photocurrent, I_{ph} vs. $10^3/T$ for four back contacts. In the thermally activated region, the I_{ph} increases almost linearly with increasing temperatures. It is produced by the thermal activation of photocarriers, following the exponential relation,

$$I_{ph} = I_0 \exp\left(\frac{-E_a}{kT}\right), \tag{4}$$

where I_0 is a prefactor, k is the Boltzmann's constant, and E_a is the activation energy. A small average activation energy value of about 15 m eV was found at low temperature ($200\,\text{K} \leqslant T \leqslant 300\,\text{K}$) for Al, Cr and ZnO/Ag back contacts. For the Ag back contact, however we have not obtained a good curve in order to calculate an activation energy. At low temperatures, the photocurrent, I_{ph} depends only weakly on temperature. I_{ph} depends linearly on the generation rate G, (Eq. (2), $\nu \approx 1$) and varies only little with the defect density or doping level. Such behavior suggests a mechanism of photoconduction which is pretty well universal and indeed quite similar behavior has been observed in many very different disordered materials [24].

At high temperatures ($300\,\text{K} \leqslant T \leqslant 360\,\text{K}$), the photocurrent is thermally enhanced. In this temperature range, an activation energy value of about 0.40 eV can be determined for the ZnO/Ag back contact only. The dependence on the generation rate, here shown by the exponent, ν, of the power-law dependence (Eq. (2)), the magnitude of I_{ph} and the kinetics are determined by the Fermi level position and the density and occupancy of the localized gap states. In other words, at high temperatures, the transport depending on the contact occurs in the extended states and the carrier lifetime is controlled, as in crystalline photoconductors, by multiple trapping mechanisms and the occupancy and capture cross-sections of the deep gap states which act as recombination centers [9].

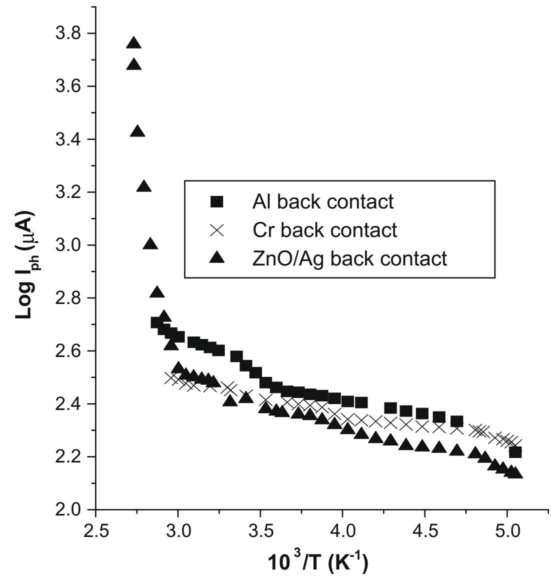

Fig. 6. A comparison of dc photocurrent vs. inverse temperature for a-Si:H p–i–n solar cell with different back contacts.

Spectral response measurements determine the wavelength dependence of the quantum efficiency (QE) of solar cell devices. The external quantum efficiency at a given wavelength is defined as the number of minority carriers collected per incident photon

$$QE(\lambda) = \frac{J_{collec}(\lambda)}{q\Gamma(\lambda)}, \tag{5}$$

where q is the electronic charge, J_{collec} is the light-generated current density resulting from monochromatic illumination, and Γ is the incident flux given by

$$\Gamma = \frac{P(\lambda \times 10^{-9})}{hc}, \tag{6}$$

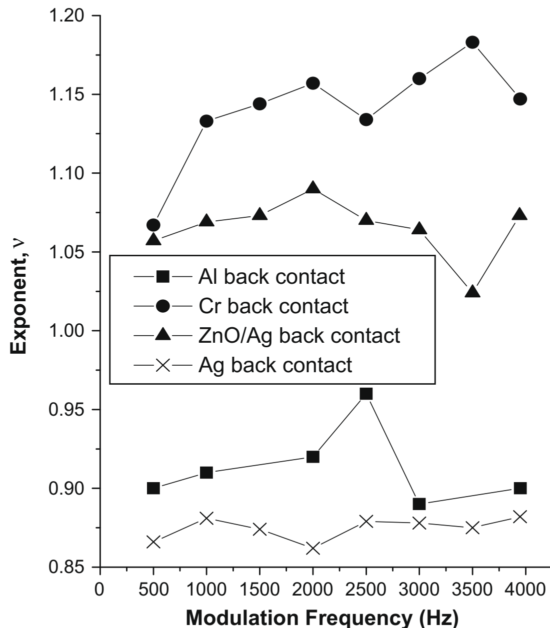

Fig. 5. The exponent ν, in the power-law $I_{ph} \propto G^{\nu}$, vs. the modulation frequency for a-Si:H p–i–n solar cell with different back contacts.

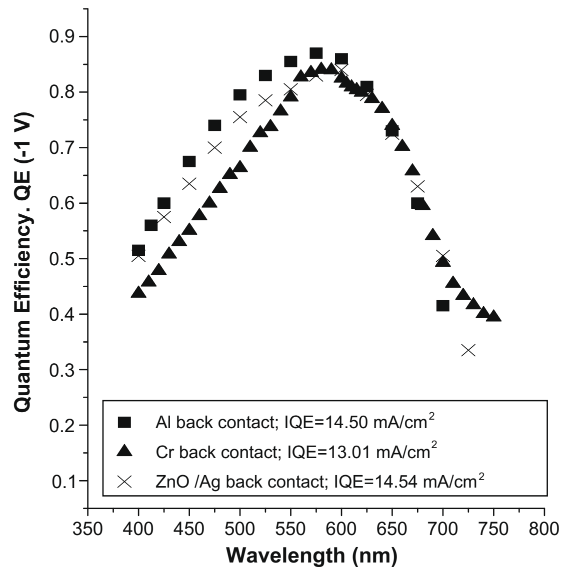

Fig. 7. A comparison of quantum efficiency, $QE(-1V)$ vs. wavelength for a-Si:H p–i–n solar cell with different back contacts. IQE stands for integrated quantum efficiency.

where P is the incident optical power density (in J s^{-1} cm^{-2}), λ is the wavelength (in nm), h is Planck's constant (in J s), and c is the velocity of light (in m s^{-1}).

$J_{collec}(\lambda)$ is a complex function of several optical and electrical device parameters. Optical device parameters include front- and back-surface reflectivity, optical distribution, absorption coefficient and total thickness. Electrical device parameters include front- and back-surface recombination velocity, p–i–n doping profiles, minority carrier diffusion length and p–i–n layer thicknesses.

The light-generated current density is calculated by integrating the product of the external quantum efficiency and the solar spectrum over wavelength

$$J_L = \int QE(\lambda)\Phi(\lambda)d\lambda, \quad (7)$$

where $\Phi(\lambda)$ is the solar spectrum expressed in mA/cm^2 $(\mu m)^{-1}$. This calculation, as in our case, is commonly performed numerically.

Fig. 7 shows a comparison of the external quantum efficiency, $QE(-1V)$ as a function of wavelength for three different back contacts. As seen, it is peaked at a wavelength near 600 nm for all back contacts. The integrated quantum efficiency (IQE) values were also shown on the plotting for all back contacts. Although IQE values are close each other, the ZnO/Ag back contact has the largest value. As seen from the figure, $QE(-1V)$ spectrum of all back contact is almost the same at longer wavelengths ($\lambda > 600$ nm).

However, at shorter wavelengths ($\lambda < 600$ nm) the values of $QE(-1V)$ for cells with Al and ZnO/Ag back contacts are larger than those of Cr back contact due to absorption of light.

Fig. 8a and b shows the modulated and dc photocurrent responses respectively, as a function of wavelength for the Cr back contact. Similar results were also observed for other back contacts. As seen, the modulation frequency and illumination intensity level have no important effects on the spectral distributions, except for magnitude. As well known, higher light intensity excitation and modulation frequency produce a larger fraction of photocarriers from deep trapping levels (defects) in the energy gap, and thus these contribute to the photocurrent.

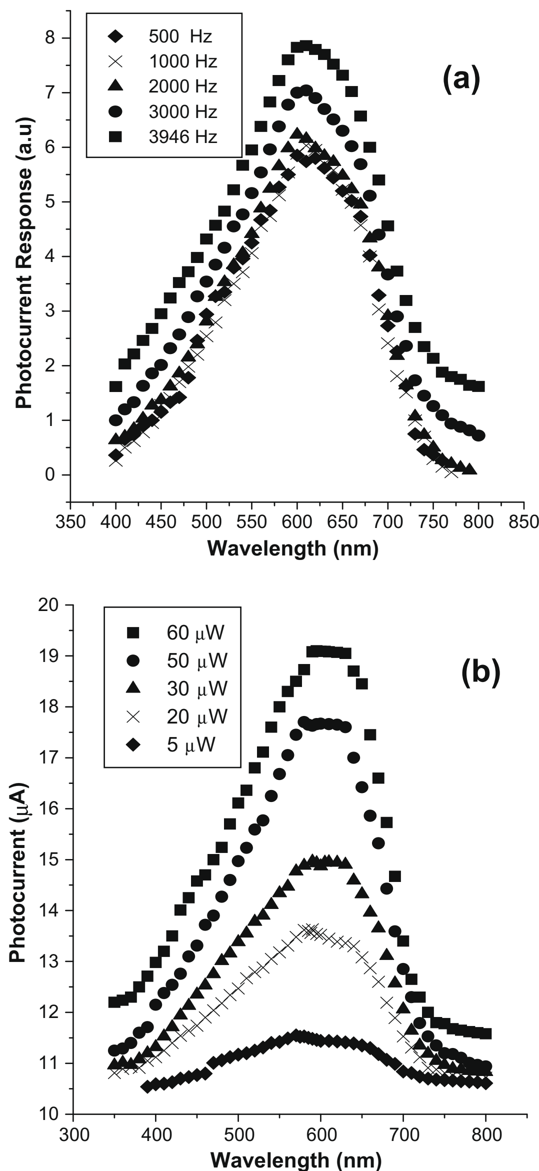

Fig. 8. Dc (a) and modulated (b) photocurrent of a-Si:H p–i–n solar cell with the Cr back contact vs. wavelength for different modulation frequencies and various illumination levels respectively.

4. Conclusion

Electrical transport and recombination mechanisms in hydrogenated amorphous silicon, a-Si:H p–i–n, are determined by localized band-tail states and deep defects. These were investigated from dc and modulated photocurrent measurements under different external conditions. We examined and compared the effects of four different back contacts (Al, Cr, ZnO/Ag and Ag) on the photocurrent response of a-Si:H p–i–n solar cells. Al back contact gives high FF, but low J_{sc}; while Cr back contact gives low FF, but high J_{sc}, under the same excitation light intensity. For the ZnO/Ag back contact, both FF and J_{sc} were found to be high and more stable. Their integrated $QE(-1V)$ values were found to be very close each other (13–14.5 mA/cm^2). However the Ag back contact lonely among them is found to be the worst for all comparisons. We must report that the modulation frequency and low illumination levels have no important effects on the spectral distributions of photocurrent, and thus $QE(-1V)$, except for magnitude.

The exponent v, in the power-low relationship $I_{ph} \propto G^{v}$, is found to be high ($v > 1$, superlinear recombination) for Cr and ZnO/Ag back contacts; while v is small, but close to 1 (monomolecular recombination) for Al and Ag back contacts. However, v is found to be almost independent of modulation frequency. On the other hand, the ZnO/Ag back contact among others gives a good activation energy value of about 0.40 eV at high temperatures. It means the photocurrent almost increases linearly with increasing temperatures.

It is well established that FF, J_{sc}, $QE(-1V)$, and the exponent v in the power-law, $I_{ph} \propto G^{v}$, are sensitive to the material of different back contacts which have influences on the cell structure. They can be improved on a-Si:H p–i–n devices by the optimization of the back contact material which acts as a reflector allowing some of the passing light to reflect into the i-layer.

Acknowledgements

We would like to thank Dr. S.S. Hegedus for supplying samples and his collaboration. This work was supported by TBAG-2212 (102T091) Contract of The Scientific and Technical Research Council of Turkey (TUBITAK), and under Mersin University Contract No. BAP-EF OFMA (RK) 2006-2.

References

[1] Smestad PG, Krebs FC, Lambert CM, Granqvist CG, Chopra KL, Mathew X, et al. Reporting solar cell efficiencies in solar energy materials and solar cells. Sol Energy Mater Sol Cells 2008;92:371–3.

[2] Minemoto T, Nagae S, Takakura H. Impact of spectral irradiance distribution and temperature on the outdoor performance of amorphous Si photovoltaic modules. Sol Energy Mater Sol Cells 2007;91:919–23.
[3] Yang J, Banerjee A, Guha S. Amorphous silicon based photovoltaics-from earth to the "final frontier". Sol Energy Mater Sol Cells 2003;78:597–612.
[4] Manea E, Budianu E, Purica M, Cristea D, Cernica I, Muller R, et al. Optimization of front surface texturing processes for high-efficiency silicon solar cells. Sol Energy Mater Sol Cells 2005;87:423–31.
[5] Mahalingam T, Join VS, Raja M, Su YK, Sebestian PJ. Electrodeposition and characterization of transparent ZnO thin films. Sol Energy Mater Sol Cells 2005;88:227–35.
[6] Mattheis J, Rostan PJ, Rau U, Werner JH. Carrier collection in Cu(In,Ga)Se_2 solar cells with graded band gaps and transparent ZnO:Al back contacts. Sol Energy Mater Sol Cells 2007;91:689–95.
[7] Hegedus SS, Kaplan R, Ganguly G, Wood GS. Characterization of the SnO_2/p and ZnO/p contact resistance and junction properties in a-Si p–i–n solar cells and modules. In: 28th IEEE PVSC; 2000. p. 728–31.
[8] Street RA. Hydrogenated amorphous silicon. Cambridge University; 1991.
[9] Fuhs W. Recombination and transport through localized states in hydrogenated amorphous and microcrystalline silicon. J Non-Cryst Solids 2008;354:2067–78.
[10] Rostan PJ, Rau U, Nguyen VX, Kirchartz T, Schubert MB, Werner JH. Low-temperature a-Si:H/ZnO/Al back contacts for high-efficiency silicon solar cells. Sol Energy Mater Sol Cells 2006;90:1345–52.
[11] Hegedus SS, Kaplan R. Analysis of quantum efficiency and optical enhancement in amorphous Si p–i–n solar cells. Prog Photovolt: Res Appl 2002;10:257–69.
[12] Hegedus SS, Buchanan WA, Eser E. Improving performance of superstrate p–i–n a-Si solar cells by optimization of n/TCO/metal back contacts. In: 26th IEEE PVSC; 1997. p. 603–6.
[13] McMahon TJ, Roeder von B. Effect of light intensity on current collection in thin-film solar cells. In: 26th IEEE PVSC; 1997. p. 375–8.
[14] Crandal RS. Modeling of thin film solar cells: uniform field approximation. J Appl Phys 1983;54:7176–86.
[15] Kaplan R. Comparative frequency-resolved photoconductivity studies of amorphous semiconductors. Sol Energy Mater Sol Cells 2005;85:545–57.
[16] Şahin M, Kaplan R. Intensity and temperature dependence of photocurrent of a-Si:H schottky diodes. Curr Appl Phys 2006;6:114–8.
[17] Kaplan B, Kaplan R. Modulation frequency-dependence of photocurrent in amorphous Si:H p–i–n and chalcogenides. Turkish J Phys 2002;26:355–62.
[18] Arene E, Baixeras J. Steady-state photoconductivity and recombination processes in sputtered hydrogenated amorphous silicon. Phys Rev B 1984;30:2016–25.
[19] Rose A. Concepts in photoconductivity and allied problems. NY: Krieger; 1978. p. 33–50.
[20] Bube RH. A new mechanism for superlinear photoconductivity with relevance to amorphous silicon. J Appl Phys 1993;74:5138–43.
[21] Hack M, Guha S, Shur M. Photoconductivity and recombination in amorphous silicon alloys. Phys Rev B 1984;30:6991–9.
[22] Morgado E. Electron and hole $\mu\tau$ products in a-Si:H and the standard dangling bond model. J Non-Cryst Solids 1993;166:627–30.
[23] Bube RH, Redfield D. Variation of photoconductivity with doping and optical degradation in hydrogenated amorphous silicon. J Appl Phys 1989;66:3074–81.
[24] Fritzsche H, Yoon BG, Chi DZ, Tran MQ. Some observations on the photoconductivity of amorphous semiconductors. J Non-Cryst Solids 1992;141:123–32.